Regular Article

PHYSICAL CHEMISTRY RESEARCH
Published by the
Iranian Chemical Society
www.physchemres.org
info@physchemres.org

Phys. Chem. Res., Vol. 10, No. 2, 293-300, June 2022
DOI: 10.22036/PCR.2021.306239.1971

Structural, Morphological, and Optical Studies of ZnS-MoS_2 Nanocomposite *via* Hydrothermal Route

K. Venkatarao[a,b], G. Sreedevi[c], Y. Nirmal Rajeev[a,d] and S. Cole[a,*]

[a]*Department of Physics, Acharya Nagarjuna University, Nagarjuna Nagar, Guntur, 522510, A.P., India*
[b]*Department of Physics, Government Polytechnic, Krosuru, Guntur, 522410, A.P., India*
[c]*Department of Physics, P.V.P. Siddhartha Institute of Technology, Vijayawada, India*
[d]*Department of Physics, V.R. Siddhartha Engineering College, Vijayawada, India*
(Received 23 September 2021, Accepted 20 November 2021)

ZnS-MoS_2 nanocomposite was synthesized by a cost-effective and eco-friendly hydrothermal method to investigate and compare the structural and optical properties of ZnS-MoS_2 nanocomposite powder with those of pure ZnS and MoS_2. The structural, morphological, and optical absorption properties of the prepared powder samples were characterized by powder X-ray diffraction (XRD), scanning electron microscopy (SEM), diffuse reflectance spectroscopy (DRS), and Fourier transform infrared (FT-IR) spectroscopy. Powder XRD results showed both cubic-phase and hexagonal-phase structures in ZnS and MoS_2. The average crystallite size varied from 20 nm to 25 nm for the hydrothermally prepared nanocomposite. The dislocation density and lattice strain were also calculated. The surface morphology of the prepared nanocomposite showed spherical, hexagonal, and flower-shaped nanoparticles with agglomeration. With the coupling of ZnS and MoS_2, a slight variation was found in the energy band gap that slightly red-shifted from 3.61 to 3.57 eV. The characteristic frequencies related to ZnS-MoS_2 nanocomposite and other related precursor molecules were determined by FT-IR spectra.

Keywords: ZnS, MoS_2, Hydrothermal method, XRD, FT-IR, DRS

INTRODUCTION

Nanotechnology is a cutting-edge technology that emerged in the twenty-first century. Manipulating the structure of materials to transform them into nanoscale structures changes their properties and leads to the development of new principles. Over the past three decades, theoretical and experimental calculations have been used to study the UV-Vis-NIR spectra of semiconductor nanoparticles due to their distinctive size-dependent properties and the quantum mechanical phenomena in semiconductors. Any variation in the size of particles can cause considerable changes in their electronic, structural, and optical properties. This is due to the three-dimensional (3-D) quantum confinement of holes and electrons that occurs when the size of the particle approaches the exciton Bohr radius, which is the separation distance between the electron and hole. Semiconductors with a tunable energy band gap are widely considered to be the materials for next-generation flat-panel displays, optoelectronic devices, sensors, photovoltaic devices, photonic band-gap devices, laser, *etc*.

Among various semiconductors, molybdenum disulfide (MoS_2), a two-dimensional transition metal dichalcogenide semiconductor with a direct band gap, has a distinctive layered structure and some unique properties, such as high electrical conductivity, high electron mobility, high chemical stability, and large surface area [1,2]. MoS_2 has several applications in the field of optoelectronics due to its excellent light absorption to the visible and IR regions. This absorption property of MoS_2 can be attributed to its band gap, which varies from around 1.3 eV to 1.8 eV [3]. In

*Corresponding author. E-mail: sandhya.cole@gmail.com

addition, the layer-dependent optoelectronic and electronic properties of MoS_2 allow the tailoring of its properties as per the required application. Notwithstanding that, MoS_2 has some shortcomings, such as quick recombination of photogenerated hole-electron pairs and slow electron transfer rate. To overcome these drawbacks, MoS_2 has been mixed with other materials having semiconducting nature to enhance its properties and increase its domain of application [4]. As regards ZnS nanophosphor, it also has some special features, such as a wide direct band gap, favorable transport properties, and high electron mobility [5]. In addition to these interesting properties, ZnS nanophosphor has adequate thermal stability and high transmittance in the infrared range, making it a promising material in optoelectronics [6]. Both ZnS and MoS_2 can be used as sulfur sources with similar lattice parameters [7]. It has been reported that ZnS-MoS_2 nanocomposite exhibited improved structural and optical properties compared with either of them individually [4]. The ZnS-MoS_2 nanocomposite has applications in both photocatalysis, due to the band gap difference in its counterparts (*i.e.*, ZnS and MoS_2), and optoelectronics, due to its wide band gap. The objective of the present study was to investigate the structural and optical properties of ZnS-MoS_2 nanocomposite powder and compare them with those of pure ZnS and pure MoS_2 nanopowders. These two compounds, namely, ZnS and MoS_2, were selected because both had wide applications in photocatalysis and optoelectronic devices. A composite containing 60% ZnS and 40% MoS_2 was used in this study since this combination was reported to have wide applications [8]. In the present work, sulfur-based ZnS-MoS_2 nanocomposite was synthesized by the hydrothermal method [9], and its structural and optical properties were characterized using different characterization techniques, including XRD, SEM, DRS, and FT-IR spectral studies.

STARTING MATERIALS AND SYNTHESIS METHOD

Materials

To prepare ZnS-MoS_2 nanocomposite powders, all chemicals with 99.9% purity were used. Sodium molybdate dihydrate ($Na_2MoO_4.2H_2O$), zinc acetate dihydrate ($C_4H_{10}O_6Zn$), thiourea (CH_4N_2S), and sodium hydroxide (NaOH) were used as starting materials. Double deionized water was used in the dilution process and sample synthesis. All the glassware used in the preparation process was cleaned with acetone.

Synthesis of ZnS-MoS_2 Nanocomposite

In this process, ZnS-MoS_2 was prepared with a 3:2 molar ratio using a single-step hydrothermal method. For this purpose, 10 mmol of CH_4N_2S, 1 mmol of $Na_2MoO_4.2H_2O$, and 1.5 mmol of Zn $(CH_3COO)_2.2H_2O$ were weighed, dissolved into 100 ml of double deionized water in a 250 ml conical flask, and stirred for 2 h using a magnetic stirrer, followed by the addition of 10 ml of 0.2 M NaOH solution drop by drop. NaOH solution was added to maintain the chemical stability at alkaline pH. After stirring, the stirred chemical was transferred into a Teflon-lining autoclave with a capacity of 150 ml, heated under autogenous pressure, placed in a hot air oven at 180 °C for 12 h, and allowed to return to room temperature for 12 h, which led to the formation of a black color precipitate. This precipitate was centrifuged at 10,000 rpm and washed four times with ethyl alcohol and double deionized water alternatively. The final precipitate was dehydrated at 120 °C for 6 h and ground with an agate mortar to obtain the powder form of the prepared ZnS-MoS_2 nanocomposite. The same procedure was followed to prepare ZnS and MoS_2 using their precursors by maintaining a 1:4 molar ratio of thiourea.

The balanced chemical equations for the synthesis processes of (1) MoS_2, (2) ZnS, and (3) ZnS-MoS_2 nanocomposites are presented below:

$$4Na_2MoO_4*2H_2O + 9CH_4N_2S + 4H_2O \rightarrow 4MoS_2 + Na_2SO_4 + 6NaOH + 9CO_2 + 18NH_3 \quad (1)$$

$$Zn(CH_3COO)_2*2H_2O + 2NaOH + CS(NH_2)_2 \rightarrow ZnS + 2CH_3COONa + 2NH_3 + CO_2 + 2H_2O \quad (2)$$

$$4Zn(CH_3COO)_2*2H_2O + 8NaOH + 4Na_2MoO_4*2H_2O + 13CS(NH_2)_2 + 4H_2O \rightarrow 4(ZnS\text{-}MoS_2) + Na_2SO_4 + 26NH_3 + 13CO_2 + 8CH_3COONa + 8H_2O + 6NaOH \quad (3)$$

CHARACTERIZATION TECHNIQUE

The nature of the prepared ZnS-MoS_2, ZnS, and MoS_2

nanopowder samples was tested at room temperature using a Rigaku MiniFlex 600 diffractometer with Cu Kα radiation (wavelength = 1.5406 Å) scanned from 3° to 90°. The dynamic reflection spectra (DRS) of the prepared samples were recorded using a UV/Vis/NIR-spectrophotometer (SPECORD-210 plus, Analytik Jena) in the region 200-1000 nm. The morphology and elemental analysis mapping of the prepared nanopowders were carried out using a JEOL JSM-IT500 scanning electron microscope (SEM) with energy dispersive X-ray analysis (EDAX). The vibrational IR spectra, in wavenumber region from 4000 to 400 cm^{-1} unit, of the prepared samples were recorded on Bruker ALPHA II model FT-IR equipment using the KBr pellet technique.

RESULTS AND DISCUSSION

Powder XRD Studies

XRD pattern was used to obtain some information about the phase purity of the prepared ZnS-MoS_2 nanocomposite powder. The recorded diffraction patterns in the range of 3° to 90° are shown in Fig. 1. The XRD pattern of ZnS-MoS_2 nanocomposite showed the presence of both cubic and hexagonal structures in ZnS and MoS_2, and the diffraction pattern peaks at 28.66°, 33.18°, 47.62°, 56.49°, 59.24°, 69.58°, 76.87°, 79.15°, and 88.62° corresponded to the lattice planes (111), (200), (220), (311), (222), (400), (331), (420), and (422) of zinc blende cubic structure of ZnS, as reported in the JCPDS card (No: 01-077-2100). In addition to the above peaks, the XRD pattern related to the ZnS-MoS_2 nanocomposite exhibited peaks at 2θ values of 26.85°, 27.26°, 28.18°, 29.21°, and 33.56°, which corresponded to the (100), (102),(103),(104), and (107) diffraction peaks of Wurtzite-10H phase of ZnS, as reported in the JCPDS card (Number: 00-012-0688). Moreover, a prominent peak at 2θ =14.02° corresponding to the (002) of the hexagonal phase of MoS_2 matched the XRD data of the standard ICDD-JCPDS card (Number: 01-075-1539) [10-12].

Undoped ZnS showed a cubic phase, but when it was coupled with MoS_2, it exhibited both cubic and hexagonal phases. Due to the coupling between ZnS and MoS_2, the cubic phase peaks intensity of ZnS decreased and the hexagonal phase peaks of ZnS increased. It can be

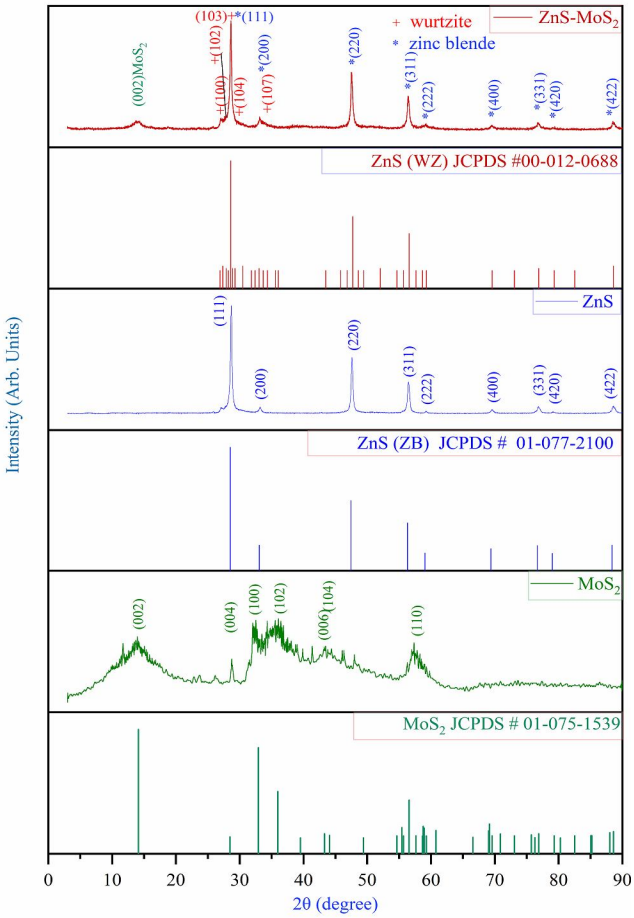

Fig. 1. The XRD pattern of ZnS, MoS_2, and ZnS-MoS_2 nanoparticles.

understood that the coupling effect heavily influenced the local distortions in the host lattice structure of the ZnS-MoS_2 sample [13]. The XRD pattern also revealed intense peaks with broad nature, which, in turn, indicates that the crystallite sizes of the synthesized powders were in the order of nanometer range. The slight shift in peak position represents strong evidence for the existence of the local disorder and lattice strain in the nanocomposite.

The mean size of the crystallite (D) can be measured from the FWHM-full width value at half maximum of intensity related to diffraction peaks. The Debye-Scherrer's equation was adapted to estimate the average crystallite size (D) of the hydrothermally prepared samples.

The widely used Debye-Scherrer's crystallite size

equation is presented below:

$$D = \frac{S_f \lambda}{(\cos\theta)\beta}$$

Here, S_f (= 0.9) is shape factor, D denotes the crystallite size, λ is the length of the wave (1.5406 Å) of the incident (Cu-Kα) X-Ray beam, β and θ (both are in radians) are the FWHM-full width value at half maximum of intensity and angle of diffraction, respectively [14].

Also, the δ-dislocation density and ε-microstrain were calculated using Williamson-Smallman relation $\delta = \frac{1}{D^2}$ and Stokes-Wilson relation $\varepsilon = \frac{\beta}{4\tan\theta}$, respectively [15]. The calculated values of crystallite size, micro-strain, and dislocation densities for the prepared samples ZnS, MoS_2, and ZnS-MoS_2 are shown in Table 1.

SEM and EDAX Studies

SEM studies were carried out to investigate surface morphologies and nanoparticle distribution of the prepared nanopowder samples under normal ambient temperature and pressure. Figure 2 shows SEM micrographs of ZnS, MoS_2, and ZnS-MoS_2 nanocomposites, respectively. While the SEM images of ZnS show hexagonal spheres, those of MoS_2 show spherical flowers type morphology. The coupling of ZnS and MoS_2 (*i.e.*, ZnS-MoS_2 nanocomposite) shows spherical hexagonal flowers with agglomerations.

The composition of MoS_2 nanoparticles, ZnS nanoparticles, and ZnS-MoS_2 nanocomposite was confirmed by the EDAX technique, which revealed the existence of the desired elements (*i.e.*, S, Mo, and Zn) in the prepared samples. Figure 3 depicts the examined EDAX patterns of the respective prepared samples.

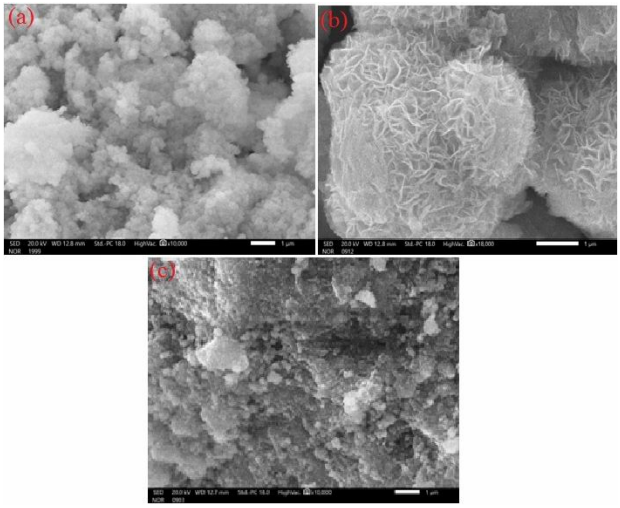

Fig. 2. The morphological SEM images of ZnS (a), MoS_2 (b), and ZnS-MoS_2 (c).

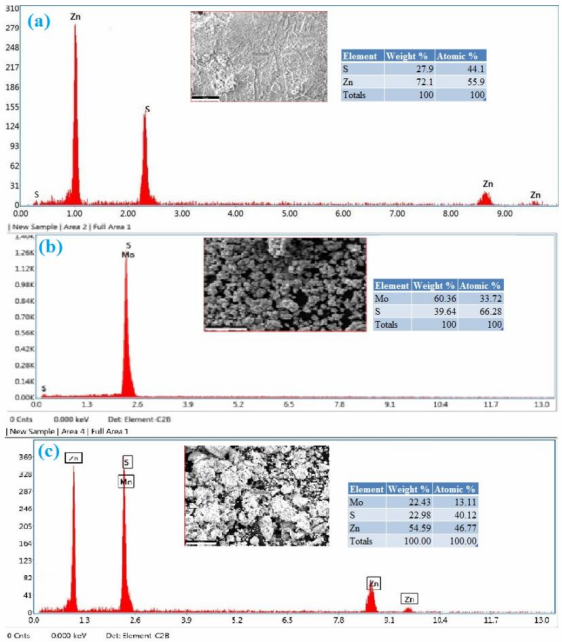

Fig. 3. The EDAX patterns of ZnS (a), MoS_2 (b), and ZnS-MoS_2 (c).

Table 1. Mean Crystallite Size, Micro-Strain and Dislocation Densities of MoS_2, ZnS, and ZnS-MoS_2 Nanoparticles

Sample	Position (2θ-degree)	FW-HM (β-degree)	Crystallite size (D) (nm)	Lattice strain [(ε) × 10^{-4}]	Dislocation density (δ) (lines/m^2)
MoS_2	14.02	0.4598	17.41	163.36	3.29×10^{15}
ZnS	28.66	0.3529	23.25	60.28	1.85×10^{15}
ZnS-MoS_2	28.60	0.4170	19.67	71.39	2.58×10^{15}

Optical Properties

DRS is a very good mechanism for samples in the powdered form as it does not require any suitable medium for measurement. The band gap calculations were performed using the observed reflection spectra from 200 to 1000 nm wavelength region. The band gap of the synthesized nanoparticles ZnS, MoS_2, and ZnS-MoS_2 were estimated using the Kubelka-Munk equation:

$$F(R) = \frac{(1-R)^2}{2R}$$

Here, R is the reflectivity of the sample.
Linear absorption coefficient α can be obtained from F(R) value by a transformation [16], as shown below:

$$\alpha = \frac{F(R)}{t} = \frac{Absorbance}{t}$$

where t is proportionality constant. Absorption co-efficient (α) and band gap (E_g) are connected by a relation
$(\alpha h\upsilon) = A(h\upsilon - E_g)^n$; $(\alpha h\upsilon) = F(R)\, h\upsilon$; $A(h\upsilon - E_g)^n = F(R)\, h\upsilon$ and
$[F(R)h\upsilon]^{1/n} = A(h\upsilon - E_g)$; here the values of n = 1/2, 3/2, 2, and 3 show allowed direct, direct forbidden, allowed indirect, and indirect forbidden transitions [17].

Figure 4 represents a graph between $(F(R)h\nu)^2$ and $h\nu$. The band gap values were extrapolated from the graph for the samples ZnS, MoS_2 (inset plot), and ZnS-MoS_2. This is an excellent method to characterize the semiconducting nanoparticles which show quantum size phenomenon due to pairs of electrons and holes generated by light [18]. The reflection spectrum in the UV-Vis region depends on the actual size of the semiconductor nanoparticles. The maxima of reflection decrease with nanoparticles size. MoS_2 with a 1.34 eV energy band gap had a NIR reflection band, and ZnS with a 3.61 eV energy band gap had an intensive UV reflection band. ZnS-MoS_2 also responded to the UV region with a 3.57 eV energy band gap, though with a redshift. The band gap values extrapolated from the graph are shown in Table 2.

FT-IR Study

To confirm the existence of precursor residuals and inspect the presence of various characteristic functional groups in MoS_2, ZnS, and ZnS-MoS_2 nanopowder samples, FT-IR measurements were performed in 400-4000 cm^{-1} range in the mode of transmittance, and their FT-IR spectra are illustrated in Fig. 5. The noticed peaks were thoroughly analyzed, and the peak positions, along with their characteristic nature, are summarized in Table 3.

At 3420 cm^{-1}, a broad dip occurred due to the O-H stretching caused by the strong interaction between H_2O and ZnS lattice surface. This happens due to the residuals of precursors during the characterization process or during the synthesis [19]. Around 2064-2080 cm^{-1}, peaks are due to -CH_2 stretching [20] and at around 1620-1637 cm^{-1} due to H-O-H bending mode [19]. The presence of H_2O was confirmed by its bending vibration at around 1620-1637 cm^{-1}.

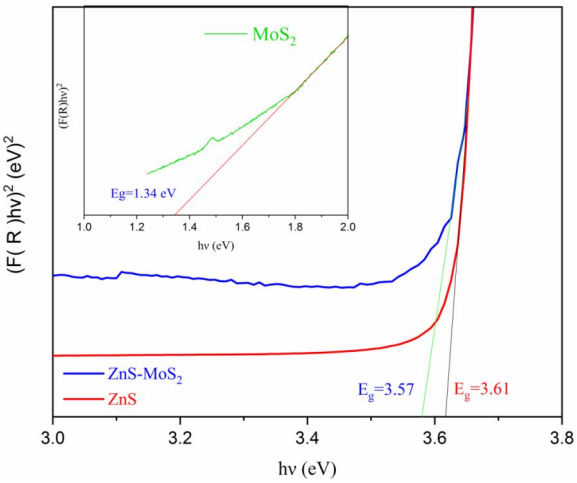

Fig. 4. The Munk plot for ZnS, MoS_2 (inset graph) and ZnS-MoS_2 nanoparticles.

Table 2. The Band Gap Values of ZnS, MoS_2, and ZnS-MoS_2 Nanoparticles

Sample code	Band gap (eV)
ZnS	3.61
MoS_2	1.34
ZnS-MoS_2	3.57

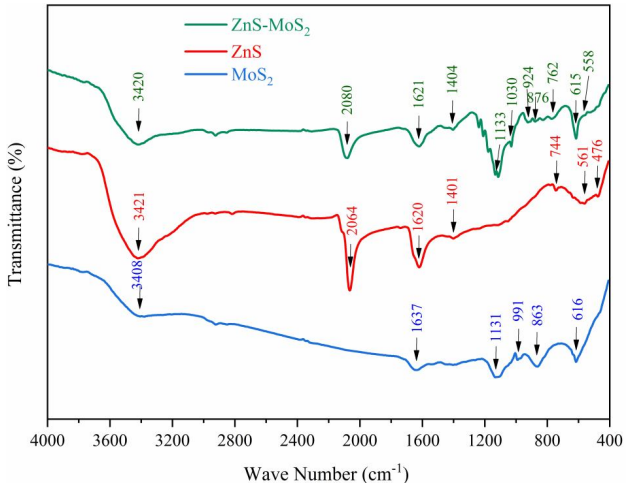

Fig. 5. The FT-IR spectra for pure ZnS, pure MoS_2, ZnS-MoS_2 nanocomposites.

Bands observed near 1404-1401 cm^{-1} can be attributed to the C-H stretching [21]. The bands located near 1133-991 cm^{-1} confirm the complex sulfur formation in MoS_2 with active sites [22]. The bands around 924, 762, 744, 558, and 476 cm^{-1} can be attributed to Zn-S vibration [23]. The bands near 876, 863, 616, and 615 cm^{-1} can be attributed to S-Mo-S vibration [24].

CONCLUSIONS

ZnS, MoS_2, ZnS-MoS_2 nanocomposites were prepared *via* a hydrothermal route. The XRD results showed that pure ZnS had both cubic (ZB) and hexagonal (WZ) phases, but when it was coupled with MoS_2, the hexagonal phase increased. The mean crystallite size of the hydrothermally synthesized nanocomposite was around 20-25 nm. The morphology of the prepared nanocomposite showed spherical hexagonal flowers with agglomerations. The coupling of ZnS-MoS_2 caused a slight energy band gap variation that red-shifted from 3.61 to 3.57 eV. FT-IR spectra revealed the possible stretching and bending vibrations modes of the prepared samples.

FUNDING

This research received no external funding.

ACKNOWLEDGMENTS

One of the authors, K. Venkatarao, would like to

Table 3. Peak Position Assignment and the Corresponding Wave Numbers in IR Spectra of ZnS, MoS_2, and ZnS-MoS_2 Nanocomposites

Vibrational frequency (cm^{-1})			Assignment of various bands
ZnS	MoS_2	ZnS-MoS_2	
476	-	-	Zn-S vibration
561	-	558	Stretching mode vibrations of Zn-S bonds
-	615	616	S-Mo-S bonds vibrations (stretching mode)
744	-	762	Stretching mode vibrations of Zn-S bonds.
-	863	876	S-Mo-S bonds vibrations (stretching mode)
-	-	924	Zn-S vibrations
-	991	1030	MoS_2 active sites
-	1131	1133	MoS_2 active sites
1401	-	1404	C-H stretching
1620	1637	1621	H_2O molecules on the particle surface
2064	-	2080	CH_2 stretching vibration
3421	3408	3420	Stretching vibration of bonded and non-bonded -O-H groups

express his deep sense of gratitude to the Department of Technical Education, Government of Andhra Pradesh, INDIA, for granting him a study leave to carry out research.

CONFLICTS OF INTEREST

The authors declare no conflict of interest.

REFERENCES

[1] Li, C.; Li, J.; Wang, Z.; Zhang, S.; Wei, G.; Zhang, J.; Wang, H.; An, C., The synthesis of hollow MoS_2 nanospheres assembled by ultrathin nanosheets for an enhanced energy storage performance. *Inorg. Chem. Front.*, **2017**, *4*, 309-314. https://doi.org/10.1039/C6QI00502K.

[2] Qin, S.; Lei, W.; Liu, D.; Chen, Y., I*n-situ* and tunable nitrogen-doping of MoS_2 nanosheets. *Sci. Rep.*, **2014**, *4*, 7582. https://doi.org/10.1038/srep07582.

[3] Wang, L.; Jie, J.; Shao, Z.; Zhang, Q.; Zhang, X.; Wang, Y.; Sun, Z.; Lee, S. -T., MoS_2/Si Heterojunction with vertically standing layered structure for ultrafast, high-detectivity, self-driven visible-near infrared photodetectors. *Adv. Funct. Mater.* **2015**, *25*, 2910-2919. https://doi.org/10.1002/adfm.201500216.

[4] Vattikuti, S. V. P.; Byon, C.; Jeon, S., Enhanced photocatalytic activity of ZnS nanoparticles loaded with MoS_2 nanoflakes by self-assembly approach. *Phys. B: Condens. Matter*, **2016**, *502*, 103-112. https://doi.org/10.1016/j.physb.2016.08.050.

[5] Fang, X.; Wu, L.; Hu, L., ZnS Nanostructure arrays: A developing material star. *Adv. Mater.* **2011**, *23*, 585-598. https://doi.org/10.1002/adma.201003624.

[6] Hussain, S.; Liu, T.; Javed, M. S.; Aslam, N.; Zeng, W., Highly reactive 0D ZnS nanospheres and nanoparticles for formaldehyde gas-sensing properties. *Sens. Actuators B Chem.*, **2017**, *239*, 1243-1250. https://doi.org/10.1016/j.snb.2016.09.128.

[7] Clark, R. M.; Carey, B. J.; Daeneke, T.; Atkin, P.; Bhaskaran, M.; Latham, K.; Cole, I. S.; Kalantar-zadeh, K., Two-step synthesis of luminescent MoS_2-ZnS hybrid quantum dots. *Nanoscale* **2015**, *7*, 16763-16772. https://doi.org/10.1039/C5NR04790K.

[8] Zhang, K.; Meng, W.; Wang, S.; Mi, H.; Sun, L.; Tao, K., One-step synthesis of ZnS@MoS_2 core-shell nanostructure for high efficiency photocatalytic degradation of tetracycline. *New J. Chem.* **2020**, *44*, 472-477. https://doi.org/10.1039/c9nj04073k.

[9] Sreedevi, G.; Srinivas, K.; Subbarao, M.; Cole, S., Investigation on structural and optical properties of CuO doped CdS-$Zn_3(PO_4)_2$ nanocomposite for optoelectronic devices. *J. Mol. Struct.* **2020**, *1222*, 128903. https://doi.org/10.1016/j.molstruc.2020.128903.

[10] Saber, M. R.; Khabiri, G.; Maarouf, A. A.; Ulbricht, M.; Khalil, A. S. G., A comparative study on the photocatalytic degradation of organic dyes using hybridized 1T/2H, 1T/3R and 2H MoS_2 nano-sheets. *RSC Adv.* **2018**, *8*, 26364-26370. https://doi.org/10.1039/C8RA05387A.

[11] Zhan, W.; Yuan, Y.; Yang, B.; Jia, F.; Song, S., Construction of MoS_2 nano-heterojunction *via* ZnS doping for enhancing *in-situ* photocatalytic reduction of gold thiosulfate complex. *Chem. Eng. J.* **2020**, *394*, 124866. https://doi.org/10.1016/j.cej.2020.124866.

[12] Zheng, J.; Zhang, R.; Wang, X.; Yu, P., Importance of carbon quantum dots for improving the electrochemical performance of MoS_2@ZnS composite. *J. Mater. Sci.* **2019**, *54*, 13509-13522. https://doi.org/10.1007/s10853-019-03860-7.

[13] Harish, S.; Prachi; Archana, J.; Navaneethan, M.; Shimomura, M.; Ikeda, H.; Hayakawa, Y., Synergistic interaction of 2D layered MoS_2/ZnS nanocomposite for highly efficient photocatalytic activity under visible light irradiation. *Appl. Surf. Sci.* **2019**, *488*, 36-45. https://doi.org/10.1016/j.apsusc.2019.05.027.

[14] Munimasthani, S.; Sarathkumar, S.; Udaychandran Thampy, U. S.; Ravikumar, R. V. S. S. N., Structural and luminescence studies of Dy3+-activated cadmium calcium pyrophosphate. *Appl. Phys. A* **2019**, *126*, 2. https://doi.org/10.1007/s00339-019-3180-x.

[15] Joyce Stella, R.; Thirumala Rao, G.; Pushpa Manjari, V.; Babu, B.; Rama Krishna, C.; Ravikumar, R. V. S. S. N., Structural and optical properties of CdO/ZnS core/shell nanocomposites. *J. Alloys Compd.*, **2015**, *628*, 39-45. https://doi.org/10.1016/j.jallcom.2014.11.201.

[16] Muswareen, S. K. K.; Rao, M. S.; Sridevi, G.; Cole, S., Sol-gel synthesis of pure and TiO_2 doped $CdOFePO_4$ nanocomposites and investigation of their structural and optical properties. *Mater. Sci. Semicond. Process.*, **2019**, *102*, 104588. https://doi.org/10.1016/j.mssp.2019.104588.

[17] Ali, H.; Mansor, E. S., Co-sensitization of mesoporous ZnS with CdS and polyaniline for efficient photocatalytic degradation of anionic and cationic dyes. *Colloids Interface Sci. Commun.*, **2020**, *39*, 100330. https://doi.org/10.1016/j.colcom.2020.100330.

[18] Stroyuk, A. L.; Kryukov, A. I.; Kuchmii, S. Y.; Pokhodenko, V. D., Quantum size effects in semiconductor photocatalysis. *Theor. Exp. Chem.*, **2005**, *41*, 207-228. https://doi.org/10.1007/s11237-005-0042-8.

[19] Ayodhya, D.; Veerabhadram, G., Facile fabrication, characterization and efficient photocatalytic activity of surfactant free ZnS, CdS and CuS nanoparticles. *J. Sci.: Adv. Mater. Devices*, **2019**, *4*, 381-391. https://doi.org/10.1016/j.jsamd.2019.08.006.

[20] Mendelsohn, R.; Flach, C. R.; Moore, D. J., Determination of molecular conformation and permeation in skin *via* IR spectroscopy, microscopy, and imaging. *Biochim. Biophys. Acta, Biomembr.*, **2006**, *1758*, 923-933. https://doi.org/10.1016/j.bbamem.2006.04.009.

[21] Mohanapriya, S.; Vennila, M.; Kowsalya, S., Synthesis and characterization of ZnS nanoparticles using Co-precipitation method. *Asian J. Appl. Chem. Res.* **2020**, *5*, 26-33. https://doi.org/10.9734/ajacr/2020/v5i130125.

[22] Zhao, D.; Wu, T.; Zhou, Y., Dual II heterojunctions metallic phase MoS2/ZnS/ZnO ternary composite with superior photocatalytic performance for removing contaminants. *Chem. Eur. J.*, **2019**, *25*, 9710-9720. https://doi.org/10.1002/chem.201901715.

[23] Tian, X.; Wen, J.; Wang, S.; Hu, J.; Li, J.; Peng, H., Starch-assisted synthesis and optical properties of ZnS nanoparticles. *Mater. Res. Bull.*, **2016**, *77*, 279-283. https://doi.org/10.1016/j.materresbull.2016.01.046.

[24] Yi, M.; Zhang, C., The synthesis of two-dimensional MoS_2 nanosheets with enhanced tribological properties as oil additives. *RSC Adv.* **2018**, *8,* 9564-9573. https://doi.org/10.1039/C7RA12897E.